Optical Engineering

OpticalEngineering.SPIEDigitalLibrary.org

Design form classification of two-mirror unobstructed freeform telescopes

Isaac Trumper
Alexander Q. Anderson
Joseph M. Howard
Garrett West
Dae Wook Kim

SPIE.

Isaac Trumper, Alexander Q. Anderson, Joseph M. Howard, Garrett West, Dae Wook Kim, "Design form classification of two-mirror unobstructed freeform telescopes," *Opt. Eng.* **59**(2), 025105 (2020), doi: 10.1117/1.OE.59.2.025105

Design form classification of two-mirror unobstructed freeform telescopes

Isaac Trumper,[a,b] Alexander Q. Anderson,[c] Joseph M. Howard,[d] Garrett West,[e] and Dae Wook Kim[a,f,*]

[a]University of Arizona, Wyant College of Optical Sciences, Tucson, Arizona, United States
[b]Intuitive Optical Design Lab LLC, Tucson, Arizona, United States
[c]University of Colorado Boulder, Department of Electrical, Computer and Energy Engineering, Boulder, Colorado, United States
[d]NASA Goddard Space Flight Center, Greenbelt, Maryland, United States
[e]Ball Aerospace, Boulder, Colorado, United States
[f]University of Arizona, Department of Astronomy and Steward Observatory, Tucson, Arizona, United States

Abstract. We present a general optical design survey of two-mirror unobstructed plane-symmetric freeform (FF) telescopes to provide a standardized framework and reference for further developments in the field of FF optics. We find that there are fundamentally two main design forms: those that use a positive tilt of the secondary and those that employ a negative rotation to achieve the unobstructed condition. Utilizing this survey, results can be categorized into simple groups of two-mirror unobstructed FF telescopes, analogous to the distinction between a Gregorian-type telescope and Cassegrain-type telescope. Allowing FF surfaces in optical design can enable more compact telescopes while potentially improving the image quality and allowing wider fields of view (FOVs). We define a FF optic as a nonrotationally symmetric mirror or lens, typically with large departures from a best-fit spherical surface (many microns or even millimeters). New manufacturing and testing methods have enabled the production of these types of surfaces. The telescopes we present maintain a 4:1 aspect ratio of the FOV and utilize X–Y polynomials for mirror surface description. We impose a plane symmetric constraint on the system and an accessible entrance pupil. We generate charts documenting the relationship between FOV and $F/\#$ for the presented optical design forms. We also compare our results to a baseline rotationally symmetric system. These results provide a general method of evaluating baseline designs for two-mirror unobstructed FF telescopes. [DOI: 10.1117/1.OE.59.2.025105]

Keywords: freeform; design survey; reflective; two mirror.

Paper 191381 received Oct. 4, 2019; accepted for publication Feb. 11, 2020; published online Feb. 27, 2020.

1 Introduction

The classification of optical design forms is an important part of developing a methodology to select the appropriate design for a given application. Most optical design texts and references place an emphasis on first choosing the design form since this classification predicts overall performance trade-offs and balances.[1,2] Design classification dictates the achievable optical capabilities of the system. Each form is distinct in how it performs, despite various similarities. Selecting a design form has far-reaching implications for the project, from fabrication to metrology. One form may have high sensitivities to manufacturing errors, whereas another may require optical elements that are hard to measure such as a large aspheric convex mirror. Therefore, exploring and developing a classification for a given design space promotes informed usage and optimal implementation of optical solutions.

*Address all correspondence to Dae Wook Kim, E-mail: letter2dwk@hotmail.com

0091-3286/2020/$28.00 © 2020 SPIE

When discussing the optical design of two-mirror on-axis telescopes, one of the first questions asked is whether it will be in a Gregorian- or Cassegrain-type configuration.[3–6] These systems have formed the backbone of many important telescopes and astronomical systems over the course of history. Since the on-axis two-mirror design forms have a well-defined classification, the trade-offs between each are clear and the insights invaluable. In this paper, we present a survey of the design space of two-mirror plane-symmetric freeform (FF) telescopes with the intention of providing insight into the classification and trade-offs that exist in these FF systems.

1.1 *Terminology Definitions*

An FF is defined here as a surface described by a general X–Y polynomial expansion but constrained to be plane-symmetric about the Y–Z plane. While the word FF typically implies having large departures from a best-fit spherical surface (many microns or even millimeters),[7] we did not constrain this departure during our work. Instead, we have focused on the extra degrees of freedom in the optical design space by using FFs, which has no constraints between different modes (e.g., Zernike terms) describing the final surface shape, unlike the off-axis conic surface with entangled and fixed ratios between the modes. Figure 1 presents an example of the difference between an FF plane-symmetric surface and rotationally symmetric (RS) surface, where the FF has significant cubic and quadratic surface signatures similar to the Zernike polynomial modes of coma and astigmatism.

1.2 *Asymmetric Optical System Design Theory*

To begin designing, a first-order layout is imperative. Bauer et al.[8] showed that, for a three-mirror plane-symmetric FF telescope, the conventional methods of choosing a starting design form are inadequate. Their methodology chooses a power balance between the mirrors and then illustrates a construction method to achieve a starting design. Further works by Papa et al.[9,10] demonstrate a robust method of surveying the three-mirror design space using Cartesian reflector starting conics. The first-order design of asymmetric optical systems (such as a two-mirror plane-symmetric FF telescope) can also be constrained using Hamilton's methods, where a single, scalar function can be used in conjunction with the ratio of indices of refraction in object and image space to completely characterize the imaging properties of the optical system.[11] Another method using an ordinary differential equation derived from the differentiation, and subsequent integration, of Fermat's path principle is also possible.[12] The configuration of the optical system can be determined with these methods to determine a set of first-order properties. Hamilton's methods were chosen in this work because it allowed us to explore the global design space more easily by not fixing a power balance before beginning the construction method.

An asymmetric optical system's first-order properties are described using geometric entities, similar to RS systems.[11,13] In general, there are 13 geometric entities that are required to specify a two-mirror plane-symmetric system. In this convention, a ray in the optical system is chosen about which to expand one of Hamilton's characteristic functions in a Taylor series, which is denoted as the "base" ray. The object, mirror, and image positions and tilts form the 13 geometric

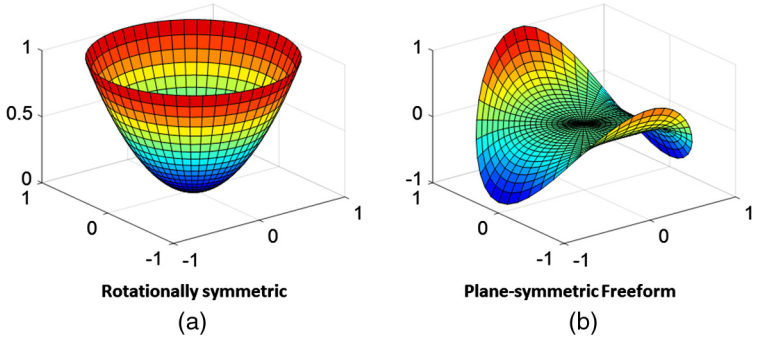

Fig. 1 Illustration of an RS surface (a) and a plane-symmetric FF surface (b). Note: All axes are normalized.

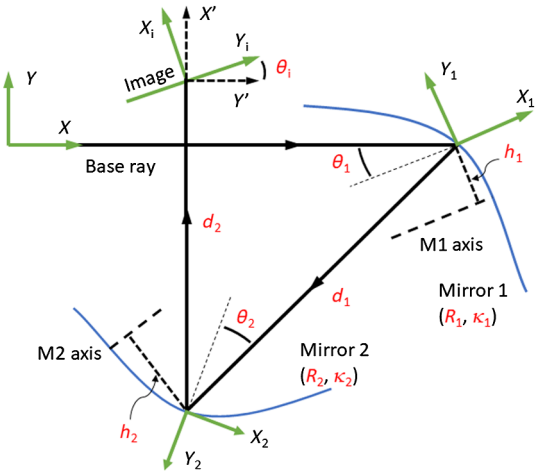

Fig. 2 Schematic diagram of a general two-mirror plane-symmetric telescope with the object at infinity. The 11 geometric parameters (in red) determine the first- and second-order image characteristics of the system,[13,14] where R and κ are the radius of curvature and conic constant, respectively.

parameters. In our situation of an object at infinity, the object plane location and tilt are defined. Figure 2 is a schematic representation of the two-mirror system with the 11 geometric parameters labeled.[14,15]

The second-order imaging properties of an asymmetric system do not necessarily vanish, which is in contrast to an RS system whose symmetry dictates they must. Thus, it is possible to even further constrain the configuration space for the system by requiring specific second-order behavior.[15] These constraints are also based on the work of Hamilton, where the Taylor series expansion is evaluated including terms of order three. This is analogous to specifying the third- and higher-order aberrations of a symmetric system and constraining them to vanish.

We are able to use the first- and second-order constraints on the imaging properties of the optical system in combination with the configuration (location and orientation of the optical elements) to generate a plane-symmetric system with two conic mirrors that forms a sharp image through second order.[15] This complete description of the second-order imaging properties simplifies the process of finding a system to suit a given application. Further analysis and optimization of the optical system found using Hamilton's method can be explained in terms of nodal aberration theory.[16–18] Interpreting the theory to provide insights in system design without closed-form constraints is also possible.[19]

1.3 *Survey Motivation*

The modern advancements in the fabrication and metrology of FF surfaces have enabled their use in realizable optical designs. However, the design space for two-mirror unobstructed FF telescopes is not well documented or classified in existing literature. We set out to perform a classification of the main design forms in this space to help future optical designers choose the correct form for their purpose. It is our hope that improved knowledge about the capabilities of these types of FF optics will facilitate their incorporation into the optical design community. We take the stance that the manufacturability of the presented designs is out of the scope of this survey, but believe it is a critical aspect to consider when evaluating a final design. Manufacturability of an FF is a function of the specific fabrication method such as single-point diamond turning, magnetorheological finishing, or computer-controlled optical surfacing,[20,21] vendor expertise, metrology method, substrate material, budget, and surface requirements among others. Of particular attention is the slope of the surface, which can be problematic when using FF surfaces. Certain FF surfaces descriptions, such as Q polynomials,[22] are formulated to provide a direct and intuitive way to estimate such characteristics. Choice of the polynomial to represent the surface should be carefully considered while also benchmarking the results of the

survey. In general, FF optics can enable a larger field of view (FOV), smaller package size, and enhanced/optimized imaging performance for optical systems. For space applications, instruments may be made in a smaller form factor, thus potentially lowering the mass and volume of a given optical system and reducing the overall cost.

1.4 *Survey Parameters*

We investigated plane-symmetric, unobstructed two-mirror imaging systems with the object at infinity. We required an unobstructed design with no vignetting for a valid comparison to current optical systems. An optimization constraint was placed on the root mean square (RMS) spot diameter, which allows for a wavelength-independent imaging performance metric to match the purely reflective systems. We maintained the FOV to have a 4:1 aspect ratio for this survey, where the larger field is orthogonal to the plane of symmetry. This is typical of push broom telescopes, where the large FOV is in the cross-track direction, and the small FOV is in the along-track direction. We assumed an accessible external entrance pupil, which allows for better stray light control and exit pupil placement. Furthermore, we specified a circular entrance pupil diameter (EPD) of 50 mm to ensure that the results of this survey are easily comparable with other similar optical systems. The EPD sets the scale for the optical system and provides a reference dimension to compare with the overall volume. We controlled the first-order anamorphism of the system by requiring that the $F/\#$ of the system in the X and Y dimensions be equal. We assumed that distortion was not a driving performance metric and could be calibrated with software. For optimization, we used X–Y polynomials with coefficients up to the 10th order for each FF surface definition but only included even terms in X (cross-track dimension) to satisfy the constraint of symmetry in the large FOV dimension. A summary of these parameters is listed in Table 1.

2 Survey Methodology

We completed this survey of two-mirror FF telescopes, aided by a set of optical constraints to ensure first- and second order image properties. We imposed these constraints when generating the starting-point optical systems using custom macros in OSLO. These constraints derive from the Hamiltonian imaging equations described by Stone and Forbes[11,13,14] and Volatier and Druart.[12]

2.1 *Design Software Platforms*

Starting designs were generated using OSLO optical design software, employing a custom macro extension called SLIDERS.[23–25] This macro essentially solves Hamiltonian imaging

Table 1 List of parameters used during the classification of the two-mirror FF telescope design forms. These parameters are tailored to space-based imaging telescopes with push broom-type FOVs.

Parameter	Specification
Optical layout	Plane-symmetric, unobstructed
Object conjugate	Infinity
FOV	4:1 aspect ratio (push broom type)
Entrance pupil	Accessible, external, 50 mm diameter
RMS spot diameter	20 μm
Telecentricity	<1 deg deviation between chief rays at image
Surface description	X–Y polynomials up to 10th order

equations in real time to define the surface for each mirror such that the desired first-order properties are met, i.e., focal length and image location, and that there is no second-order blur at the center of the field. The surface prescriptions for these FF mirror surfaces are then applied and higher-order surface coefficients are locally optimized over the desired FOV. The systems are then exported to CODE V to further optimize and generate the final telescope prescriptions. Finally, MATLAB was used to import CODE V data to perform further analysis and create plots/graphs.

2.2 *First-Order Specifications*

To maintain a circular exit pupil during optimization, we controlled the working $F/\#$ of each design in both the X and Y dimensions, in and out of the plane of symmetry. For a given EPD, this is equivalent to specifying the effective focal length (EFL) of the optical system along each axis. The $F/\#$ in an FF optical system is set by the angle between the rays at the edge of the pupil in the X and Y directions for the X and Y $F/\#$s, respectively. Therefore, by calculating the angle by means of a dot product between the direction cosines of these edge rays, a real $F/\#$ is calculated, as shown in Eqs. (1) and (2),

$$\cos\,\theta = \hat{r}_1 \cdot \hat{r}_2 = L_1 * L_2 + M_1 * M_2 + N_1 * N_2, \tag{1}$$

$$F/\# = \frac{1}{2\,n\,\sin\,\theta/2}, \tag{2}$$

where L_i, M_i, and N_i are the direction cosines of the ray used to compute the $F/\#$ and θ is the angle between the rays.

A schematic representation of the real $F/\#$ found from the ray data is given in Fig. 3. The real ray method of specifying the EFL also ensures that there is no confusion about where or how the focal length is measured. Rather it is defined in the conventional manner of taking the product of the $F/\#$ and the EPD. In general, when using FF optics in plane-symmetric systems, real ray-based quantities are required for verifying the first-order parameters. However, the first-order specifications for the starting point designs are set by the equations that control the EFL and back focal length (BFL), which are termed the parabasal equations. These can be compared to the paraxial equations for RS systems.

2.3 *Optical Specifications*

We used a grid of points to sample the FOV where the plane symmetry in the X dimension was leveraged such that only a half grid of the full field of view (FFOV) is required to adequately sample the optical system. We specified both positive and negative field points in the Y direction,

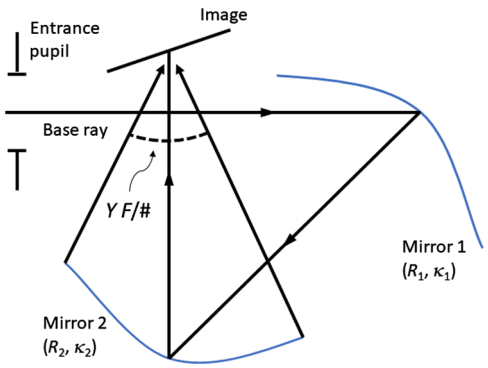

Fig. 3 Illustration of the real rays used in calculating the $F/\#$ of the system in the X direction to control anamorphism of the pupil. Similar rays are used in the Y direction. The parabasal equations that determine the EFL and BFL set the first-order parameters.

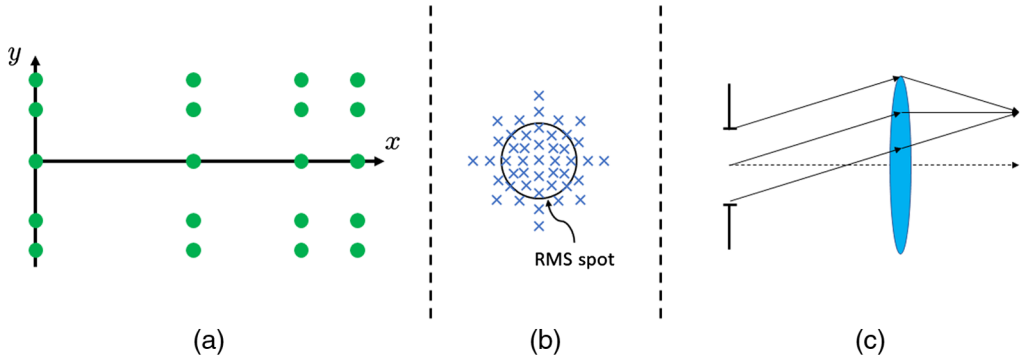

Fig. 4 Illustration of (a) the plane-symmetric field sampling employed in the survey, (b) imaging performance metric of the RMS spot diameter found by real ray locations, and (c) a telecentric optical system diagram showing the exit pupil imaged to infinity, which was constrained in the optimization.

whereas we only used positive field points in the X direction. We set the largest field in the X direction to be four times the largest field in the Y direction in order to maintain the $4:1$ FOV aspect ratio set in Table 1. In this way, the large FOV is symmetric and not in the plane where the design has anamorphism. This field sampling is shown schematically in Fig. 4(a). We define five reference rays for each field point that correspond to the ray in the center of the pupil (chief ray), and a ray at each edge of the pupil in the $+X$, $-X$, $+Y$, and $-Y$ directions. We used these ray definitions in our analysis and optimization for some custom constraints. In subsequent sections, they will be referred to as the reference rays.

In this work, each system was compared using the imaging performance metric of the worst-case RMS spot diameter over a given FOV, for a particular working $F/\#$. A specification of 20-μm RMS spot diameter was chosen to compare each design, where the extent of the field was varied for a given working $F/\#$ to meet the image quality target. The RMS spot diameter is computed from real ray data and is a geometric quantity, as depicted in Fig. 4(b).

We also investigated a constraint on the telecentricity of the image space of the optical system, represented schematically in Fig. 4(c). The telecentric constraint was to have less than 1 deg of angular deviation between chief rays for all field points at the image. We impose this constraint by taking the dot product between the direction cosines of the chief rays for each evaluated field point of the optical system and calculate the maximum angle between them.

Knowledge about how the FOV, $F/\#$, and spot diameter correlate to the volume for a given design class is useful for determining what type of telescope to implement for a given application. We recorded a volume for each design such that the spot diameter, FOV, and $F/\#$ could be compared with one another with this in mind. Note that no volume constraint was applied during optimization. To compute the volume estimate, we obtained the global coordinates of all five reference rays at each surface as they propagated through the optical system. Then we evaluated the maximum and minimum values of the rays in each spatial direction, resulting in the dimensions of a rectangular box that encompasses the optical system. A volume is then computed by multiplying these values together. This volume estimate does not include a mirror thickness or a mechanical structure to mount the mirrors. It is meant as a comparison between design forms more than an estimate of the actual system volume.

2.4 *Optimization Methods*

We explored the design space of the two-mirror FF telescopes in a systematic manner by varying the $F/\#$ and FOV while maintaining an imaging performance requirement. We used two distinct methods to account for variances in optimization. The first method we used to accomplish this was to set the $F/\#$ at a constant value while increasing or decreasing the FOV and reoptimizing until the imaging performance metric was met. If the performance exceeded the requirement, we increased the FOV until the limiting case was found. Then, we would increment the $F/\#$.

To generate a smooth enough curve while being efficient, we generally implemented an $F/\#$ step size between 0.25 and 0.5. For designs that were unstable during optimization, we lowered the step size but, in general, the FF designs were able to accommodate large jumps in both the FOV and $F/\#$ and still optimize well. The other method we used samples the FOV in specific intervals and iterates the $F/\#$ along with optimization to meet the imaging requirement. For this method, we used an FOV step size of approximately 1 deg. Similar to the first method of exploring, the designs were generally amicable to large jumps in FOV and $F/\#$. Throughout the survey, we used both styles and garnered equivalent results. At the start of the survey, to test that our methods were sound, we used the same starting point design to explore a space and ended up with nearly identical results. We attribute this to the fact that the two-mirror design space is small enough such that any reasonably thorough method of optimization will result in the same design.

2.5 *Baseline Comparison*

We designed an optical system that uses purely RS surfaces under the same constraints as the FF systems such that we could directly compare the FOV, $F/\#$, spot size, and volume. The RS system is of a Cassegrain-like form, with a positive powered primary mirror. We imposed a common axis of rotational symmetry on the system, but to meet the unobscured requirement, we allowed off-axis sections of the mirrors and a field bias or tilt of the first surface. To make sure that we were comparing the RS designs to the FF designs fairly, we allowed the image plane to tilt as well. The surfaces used are general aspheres, where we utilized up to 10th-order polynomials. Both nontelecentric RS optical systems and telecentric systems are reported.

3 Telescope Design Form Classification Using Folding Direction

The design space encompassed by the systems we investigated is vast. The sheer number of variables in an FF optical system can create a confusing, chaotic, and difficult-to-explain design. However, we found that amid a haze of data and parameters, two main design forms shone through. The distinguishing feature we use to classify the two-mirror unobstructed FF telescopes investigated in this work is the folding direction created with the secondary mirror. This classification uses the system geometry to distill and categorize the traits of an FF optical design in an elegant and intuitive way. In this manner, a visual and obvious feature of the system is employed to gain intuition around the optical performance.

Classification methods employed in axially symmetric design spaces are typically focused on the optical power and its grouping throughout the design. However, we find that the power of the mirrors correlates strongly with the folding direction but is not as significant of a classifying factor. Therefore, we include this as a secondary distinction.

3.1 *Two Design Forms: Type 4 and Type Z*

We define a central ray, or base ray, which passes through the center of the field and pupil in the plane of symmetry. This ray is used to specify the geometry in the optical system, such that the mirrors are centered on this ray and their tilts are taken about the base ray intersection point or basal point of the mirror. All tilts in the system are about the X axis, such that the system can be viewed accurately by looking at a projection into the YZ plane. A 0-deg tilt corresponds to the surface normal aligned to the base ray (from the previous surface) at the basal point. For a general two-mirror telescope, there are two distinct folding directions to achieve an unobstructed design. These two forms are illustrated in Fig. 5. We differentiate between these forms by the sign of the tilt angle on the secondary mirror. The sign convention employed here is that a positive angle corresponds to a counter-clockwise rotation while a negative angle describes a clockwise rotation. Only positive tilts on the first mirror are required due to symmetry.

When the secondary mirror is tilted about the X axis by a positive angle with respect to the basal point, we achieve a geometry where the light is folded back toward the incoming beam

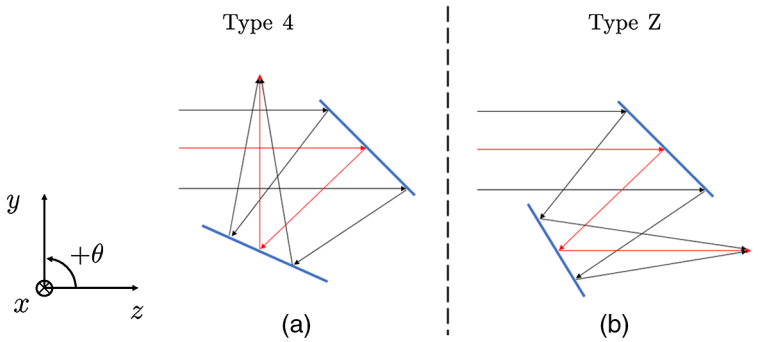

Fig. 5 Illustration of the two design forms used to categorize the two-mirror FF design space (a) type 4, and (b) type Z. The type 4 design form uses only positive tilts about the *x* axis, whereas the type Z design form has a negative tilt on the second mirror.

path. To achieve an unobstructed design, this typically means the image plane is placed on the far side of the incident beam from the secondary. In this configuration, the design resembles the numeral 4, hence we have termed it a "type 4" form, representing the positive sign of the tilt angle about the *X* axis for each mirror. In the case that the secondary has a negative folding angle, opposite from the type 4 case, the light is reflected in the same general direction as the incoming beam. In this layout, it closely resembles the letter Z, which inspired the naming of "type Z." Figure 6 shows the two-dimensional cross sections (in the plane of symmetry) of nine representative designs selected from this work, highlighting the diversity of design forms in this solution space.

Prescriptions for a type Z, type 4, and RS design at $F/5$, which are representative of how the survey systems were defined, are given in tabular form in Sec. 6 for reference.

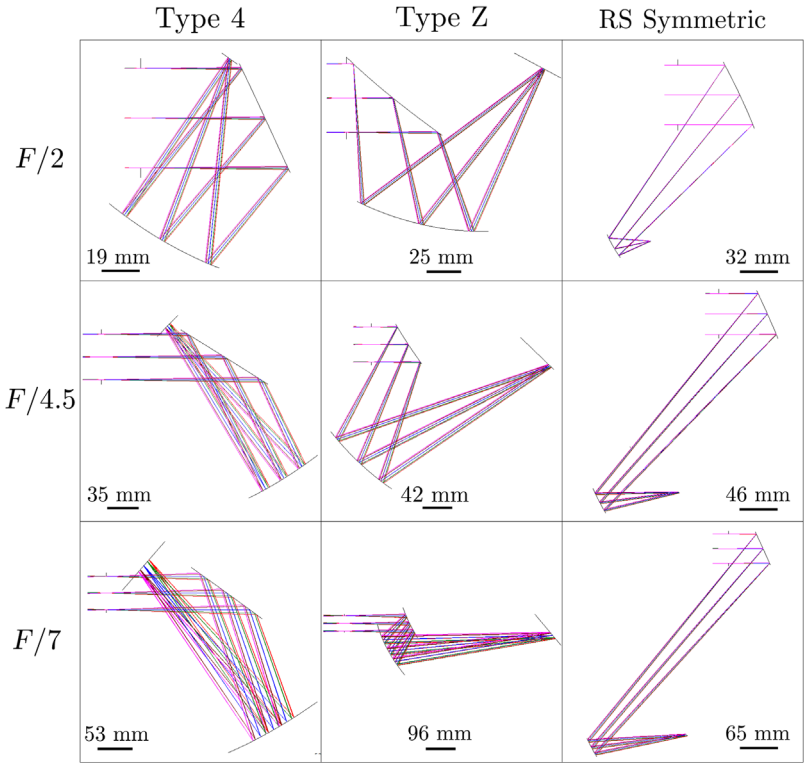

Fig. 6 Design categories of two-mirror FF telescopes sampled at three representative $F/\#$s to provide a general design layout insight for each category and a visual estimate of the volume of the optical system.

4 Optical Performance Analysis and Evaluation

4.1 *Trade-off Space between Field of View and* F/#

Important optical specifications such as FOV, $F/\#$, and system volume are affected by the choice of design form. We report the relationship found between these three characteristics for the two classifications of two-mirror FF telescopes we investigated. A FOV versus $F/\#$ curve is generated, similar to a bubble diagram shown in many optical design texts,[26] which is shown in Fig. 7. This curve allows optical engineers and scientists to quickly downselect and decide if a baseline design form, such as the type 4 or type Z, is worth investigating for a specific application.

For a nontelecentric optical system, the type Z design achieves the largest FOV for all $F/\#$s compared to the type 4 and RS baseline. In the telecentric case, at $F/\#$s greater than $F/4.5$, the type 4 design performs better than the type Z, whereas for smaller $F/\#$s, they perform similarly. The type 4 design form also obtains a larger FOV than the RS baseline system for both a telecentric and nontelecentric case, highlighting the benefits of utilizing an FF surface in optical design of off-axis unobstructed systems. In the nontelecentric case, the type 4 and type Z design forms follow an approximately parabolic relationship between the FOV and $F/\#$ for a fixed spot diameter imaging requirement. The relationship in the telecentric case is not quite as clear, where an inflection point was found around $F/5$ for both design forms.

4.2 *Trade-off Space between Volume and* F/#

When we examine the volume of the system versus $F/\#$, which can be a critical parameter for space-based telescopes, the type Z design has a significantly larger spatial extent than all other design forms, as shown in Fig. 8.

A strong trade-off between optical performance and volume exists for the type Z design form. When a telecentric constraint is imposed, the volume is reduced to a more manageable size, but the performance difference between the type 4 and type Z is also minimal. The type 4 design form maintains a smaller volume than the RS design while achieving a better FOV.

4.3 *Discussion of the Field of View and Volume for the Two Design Forms*

The type Z system closely resembles a Schwarzschild design, which has a negative-powered primary mirror and a large positive-powered secondary. This design form is well known for

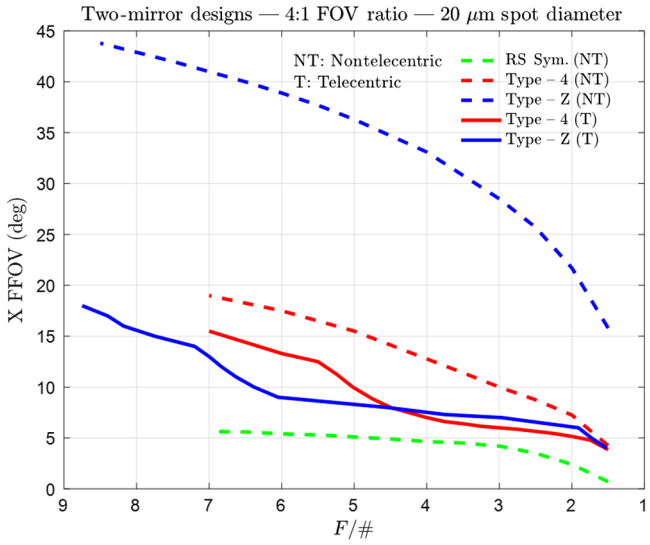

Fig. 7 FFOV in the direction of symmetry (X) versus $F/\#$ for the various design forms and telecentricity constraints investigated in this survey. Solid lines denote the telecentric systems (<1 deg deviation between chief ray angles at image plane), and dashed lines refer to no telecentricity constraint. The type Z design form provides significantly superior optical performance (FOV and $F/\#$) compared to the RS, type 4, and type Z in the nontelecentric case.

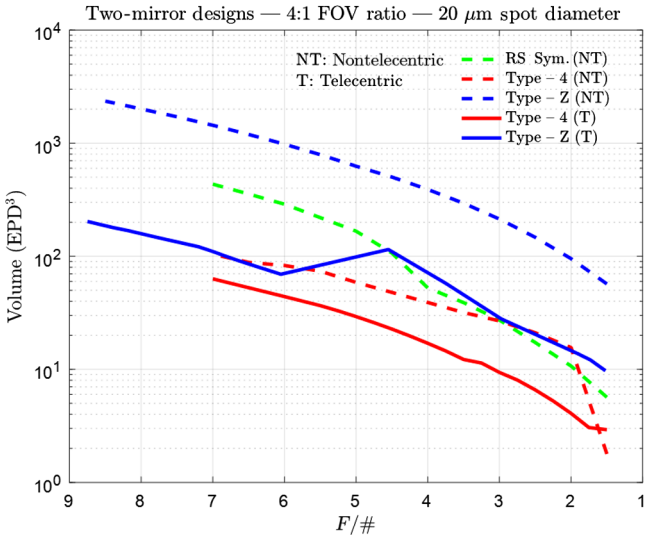

Fig. 8 Plot of the system volume in log-space versus $F/\#$ for all types of two-mirror FF telescopes investigated in this work. Solid lines denote the telecentric systems (<1 deg deviation between chief ray angles at image plane), and dashed lines refer to no telecentricity constraint. Note that the FOV varies as a function of $F/\#$. While the type Z obtains the largest FOV, it comes at the cost of system volume. The type 4 design form is a more balanced optical configuration, performing significantly better than its RS counterpart while keeping the same or smaller volume.

obtaining large FOVs,[6,27] which is exactly the behavior we observe in the FF design. When two positive-powered mirrors are used to form an image, the Petzval field curvature degrades image quality rapidly with field angle. With a negative primary, it is able to balance the Petzval, and therefore maintain image quality for larger FOVs. The downside with this approach is that the secondary mirror diameter must increase to accept the light reflected off of the negative primary. Therefore, the Schwarzschild-like designs suffer from large volumes as we see in the type Z design. A Schwarzschild-like design for the type 4 geometry is not as beneficial because the positive tilt angle of the secondary creates larger angles of incidence on the mirror, which increases the magnitude of the aberrations. Therefore, a type 4 design form that tries to balance the Petzval creates more problems in the form of other aberrations.

4.4 *Telecentric versus Nontelecentric System Design*

Comparing a telecentric with a nontelecentric design, within the same design form, the telecentric FF systems do not achieve as large FOVs for any $F/\#$. The telecentric FF systems do have smaller volumes for a majority of $F/\#$s compared to the nontelecentric designs. This is because the entrance pupil wants to be close to the first mirror. When the telecentricity constraint is released, the entrance pupil shifts away from the mirrors, which results in a larger volume, as shown in Fig. 8.

A unique feature about the telecentric systems is that for large $F/\#$s, the type 4 design performs better and has a smaller volume than the type Z design form, whereas at small $F/\#$s, the type Z design performs slightly better, although it has a larger volume. This crossover behavior is explained by the type 4's change of design space. At small $F/\#$s, the tilts of the primary and secondary mirrors are small, but at large $F/\#$s, the tilt of the primary mirror increases significantly.

4.5 *Two-Mirror versus Three-Mirror Telescope Solution Spaces*

In general, the three-mirror designs that have been surveyed previously can achieve better optical performance (spot size, FOV, distortion, etc.) at the expense of another optical surface. This leads to typically larger volumes and more complex fabrication and testing. For this reason, choosing the appropriate design form has more impacts than just optical and should be carefully evaluated.

5 Concluding Remarks

In the application space of two-mirror, unobstructed, plane-symmetric FF telescopes with the object at infinity, there exists two distinguished main design forms: type 4 and type Z. Each design form has trade-offs, where the type Z can achieve very large FOVs, but its system volume is also large. Furthermore, FF surfaces show a significant improvement in the achieved FOV over RS surfaces.

As the $F/\#$ decreases to a value of 2, the volumes of both design forms converge. This is because the EFL of the optical system becomes a significant fraction, one-half, of the entrance pupil. Therefore, the rays must be focused quickly, which brings the mirrors closer together and reduces the total volume of the optical system.

While optimizing each system, we noted the following characteristics. A telecentricity constraint generally made the optimization less stable for both design forms, but especially for the type Z geometry. The other significant trend that we noticed was that the imaging performance of the design often decreased when an X–Y polynomial order of greater than 6 or 7 was used. We believe that this is a software issue, where the optimizer is not set up properly to control so many polynomial terms. Therefore, when all the coefficients up to 10th order are allowed to vary, the optimizer actually walks away from the minimum.

Further work in the area of surveying the design solution space for two-mirror plane-symmetric FF telescopes is still needed. The manufacturability of the surfaces, the imaging performance as a function of FOV and/or volume, and evaluation of different surface equations/parameters are all potent and important avenues to explore. The multitude of constraints and considerations for various applications of an optical system leave much work for optical designers looking to find a good starting design form.

6 Appendix A

Prescriptions for an RS (Table 2), type Z (Table 3), and type 4 (Table 4) design at $F/5$, which are representative of how the survey systems were defined in this study, are given in tabular form for reference. The tables contain the type of each surface, a label, and the optical parameters needed to recreate the system. Thicknesses are with respect to the previous surface, and any parameter omitted is zero. All length units are in millimeters and angle units are in degrees.

6.1 F/5 Rotationally Symmetric Design Prescription

Table 2 $F/5$ RS design prescription.

Surface	Surface type	Radius	Conic	Thickness
Object	N.A.	0	0	Inf.
Stop	Sphere	0	0	608.72
M1	Asphere	−4573.12	606.6	−489.35
M2	Asphere	444.97	−1.7	177.66
Image	Sphere	0	0	N.A.
Asphere coefficients				
Order	4th	6th	8th	10th
M1	2.14E-09	−7.93E-14	7.66E-18	−2.36E-22
M2	2.31E-09	1.43E-15	−6.39E-20	1.14E-24
Decenters/tilts				
	X	Y	Z	Alpha	Beta	Gamma
M1	0	0	0	19.96	0	0
M2	0	0	0	0	0	0
Image	0	0	0	24.51	0	0

6.2 F/5 Type Z Design Prescription

Table 3 $F/5$ type Z design prescription.

Surface	Surface type	Radius	Conic	Thickness
Object	N.A.	0	0	Inf.
Stop	Sphere	0	0	351.46
M1	$X-Y$ polynomial	0	0	−139.88
M2	$X-Y$ polynomial	0	0	196.82
Image	Sphere	0	0	N.A.

$X-Y$ polynomial coefficients						
M1	x^2	y^2	x^2y	y^3	x^4	x^2y^2
	−0.00048	−3.09E-04	4.21E-07	2.79E-07	7.12E-10	−1.97E-10
	y^4	x^4y	x^2y^3	y^5	x^6	x^4y^2
	−1.08E-09	1.83E-11	2.99E-12	1.81E-12	−2.59E-13	−8.44E-13
	x^2y^4	y^6	x^6y	x^4y^3	x^2y^5	y^7
	−5.75E-14	8.27E-13	−4.54E-15	5.70E-15	5.61E-16	−9.09E-16
	x^8	x^6y^2	x^4y^4	x^2y^6	y^8	x^8y
	5.99E-17	2.18E-16	1.31E-16	−6.71E-17	−3.15E-16	6.67E-19
	x^6y^3	x^4y^5	x^2y^7	y^9	x^{10}	x^8y^2
	−9.20E-19	−4.51E-19	2.04E-19	2.08E-19	−3.66E-21	−1.20E-20
	x^6y^4	x^4y^6	x^2y^8	y^{10}	—	—
	−2.51E-20	−4.79E-21	1.85E-20	4.39E-20	—	—
M2	x^2	y^2	x^2y	y^3	x^4	x^2y^2
	0.000837	0.000723	1.50E-06	1.32E-06	1.95E-09	2.39E-09
	y^4	x^4y	x^2y^3	y^5	x^6	x^4y^2
	2.46E-10	4.22E-11	1.50E-11	6.31E-12	−2.87E-13	−1.28E-12
	x^2y^4	y^6	x^6y	x^4y^3	x^2y^5	y^7
	−2.54E-13	2.48E-12	−9.84E-15	8.10E-15	−2.16E-15	−2.33E-15
	x^8	x^6y^2	x^4y^4	x^2y^6	y^8	x^8y
	4.70E-17	2.40E-16	2.90E-16	−1.92E-16	−1.61E-15	1.04E-18
	x^6y^3	x^4y^5	x^2y^7	y^9	x^{10}	x^8y^2
	−1.52E-18	−6.21E-20	1.20E-18	5.77E-19	−2.15E-21	−8.38E-21
	x^6y^4	x^4y^6	x^2y^8	y^{10}	—	—
	−4.72E-20	2.48E-21	6.68E-20	3.78E-19	—	—

Decenters/tilts						
	X	Y	Z	Alpha	Beta	Gamma
M1	0	0	0	36.64	0	0
M2	0	0	0	21.79	0	0
Image	0	0	0	4.07	0	0

6.3 F/5 Type 4 Design Prescription

Table 4 $F/5$ type 4 design prescription.

Surface	Surface type	Radius	Conic	Thickness
Object	N.A.	0	0	Inf.
Stop	Sphere	0	0	57.08
M1	$X-Y$ polynomial	0	0	−504.02
M2	$X-Y$ polynomial	0	0	571.34
Image	Sphere	0	0	N.A.

$X-Y$ polynomial coefficients						
M1	x^2	y^2	x^2y	y^3	x^4	x^2y^2
	0.000767011	5.19E-04	−5.89E-07	−4.14E-07	2.94E-09	3.77E-09
	y^4	x^4y	x^2y^3	y^5	x^6	x^4y^2
	1.77E-09	−3.43E-11	−3.11E-11	−2.94E-12	−1.65E-13	−3.29E-14
	x^2y^4	y^6	x^6y	x^4y^3	x^2y^5	y^7
	3.49E-15	−6.18E-14	6.57E-15	1.13E-14	3.10E-15	−1.17E-15
M2	x^2	y^2	x^2y	y^3	x^4	x^2y^2
	0.000719818	0.000711	−1.24E-07	−1.22E-07	4.08E-10	8.56E-10
	y^4	x^4y	x^2y^3	y^5	x^6	x^4y^2
	4.43E-10	−2.29E-13	−4.56E-13	−2.53E-13	5.92E-16	1.92E-15
	x^2y^4	y^6	x^6y	x^4y^3	x^2y^5	y^7
	2.09E-15	7.51E-16	−7.75E-19	−2.85E-18	−1.84E-18	−1.42E-18

Decenters/tilts						
	X	Y	Z	Alpha	Beta	Gamma
M1	0	0	0	34.51	0	0
M2	0	0	0	−6.3	0	0
Image	0	0	0	−27.27	0	0

Acknowledgments

The authors would like to acknowledge the support of the II-VI Foundation, and the employees and mentors at Goddard Space Flight Center who helped and guided this design space investigation project. The authors have no competing interests to declare.

References

1. J. Bentley and C. Olson, *Field Guide to Lens Design*, SPIE Press, Bellingham, Washington (2012).
2. R. R. Shannon, *The Art and Science of Optical Design*, Cambridge University Press, Cambridge (1997).
3. C. L. Wyman and D. Korsch, "Aplanatic two-mirror telescopes: a systematic study. 1: Cassegrainian configuration," *Appl. Opt.* **13**, 2064–2066 (1974).

4. C. L. Wyman and D. Korsch, "Systematic study of aplanatic two-mirror telescopes. 2: The Gregorian configuration," *Appl. Opt.* **13**, 2402–2404 (1974).
5. C. L. Wyman and D. Korsch, "Aplanatic two-mirror telescopes; a systematic study. 3: The Schwarzschild–Couder configuration," *Appl. Opt.* **14**, 992–995 (1975).
6. W. B. Wetherell and M. P. Rimmer, "General analysis of Aplanatic Cassegrain, Gregorian, and Schwarzschild telescopes," *Appl. Opt.* **11**, 2817–2832 (1972).
7. K. P. Thompson and J. P. Rolland, "Freeform optical surfaces: a revolution in imaging optical design," *Opt. Photonics News* **23**(6), 30–35 (2012).
8. A. Bauer, E. M. Schiesser, and J. P. Rolland, "Starting geometry creation and design method for freeform optics," *Nat. Commun.* **9**, 1756 (2018).
9. J. C. Papa, J. M. Howard, and J. P. Rolland, "Three-mirror freeform imagers," *Proc. SPIE* **10690**, 106901D (2018).
10. J. C. Papa, J. M. Howard, and J. P. Rolland, "Starting point designs for freeform four-mirror systems," *Opt. Eng.* **57**(10), 101705 (2018).
11. B. D. Stone and G. W. Forbes, "Foundations of first-order layout for asymmetric systems: an application of Hamilton's methods," *J. Opt. Soc. Am. A* **9**, 96–109 (1992).
12. J.-B. Volatier and G. Druart, "Differential method for freeform optics applied to two-mirror off-axis telescope design," *Opt. Lett.* **44**(5), 1174–1177 (2019).
13. B. D. Stone and G. W. Forbes, "Characterization of first-order optical properties for asymmetric systems," *J. Opt. Soc. Am. A* **9**, 478–489 (1992).
14. B. D. Stone and G. W. Forbes, "Foundations of second-order layout for asymmetric systems," *J. Opt. Soc. Am. A* **9**, 2067–2082 (1992).
15. B. D. Stone and G. W. Forbes, "Second-order design methods for definitive studies of plane-symmetric, two-mirror systems," *J. Opt. Soc. Am. A* **11**, 3292–3307 (1994).
16. L. B. Moore, A. M. Hvisc, and J. Sasian, "Aberration fields of a combination of plane symmetric systems," *Opt. Express* **16**, 15655–15670 (2008).
17. K. P. Thompson, "Description of the third-order optical aberrations of near-circular pupil optical systems without symmetry," *J. Opt. Soc. Am. A* **22**, 1389–1401 (2005).
18. K. Fuerschbach, J. P. Rolland, and K. P. Thompson, "Theory of aberration fields for general optical systems with freeform surfaces," *Opt. Express* **22**(22), 26585–26606 (2014).
19. B. D. Stone and J. M. Howard, "Low-order aberration coefficients applied to design of telescopes with freeform surfaces," *Proc. SPIE* **10562**, 1056229 (2017).
20. B. Ma et al., "Applying slope constrained Q-type aspheres to develop higher performance lenses," *Opt. Express* **19**, 21174–21179 (2011).
21. N. Takaki, A. Bauer, and J. P. Rolland, "On-the-fly surface manufacturability constraints for freeform optical design enabled by orthogonal polynomials," *Opt. Express* **27**, 6129–6146 (2019).
22. G. W. Forbes, "Characterizing the shape of freeform optics," *Opt. Express* **20**, 2483–2499 (2012).
23. J. M. Howard, "Optical design using computer graphics," *Appl. Opt.* **40**, 3225–3231 (2001).
24. J. M. Howard, "Optical design tools for reflective optical systems," *Proc. SPIE* **4849**, 407–412 (2002)
25. J. M. Howard, "SLIDERS: the next generation of automated optical design tools has arrived," *Proc. SPIE* **5174**, 19–25 (2003).
26. W. J. Smith, *Modern Lens Design*, McGraw-Hill, New York (2005).
27. J. M. Sasian, "Design of a Schwarzschild flat-field, anastigmatic, unobstructed, wide-field telescope," *Opt. Eng.* **29**(1), 1–5 (1990).

Isaac Trumper received his PhD from the University of Arizona, focusing on software tools for freeform metrology, design, and analysis. He is now CTO at ELE Optics, developing the next generation of software for light-based technology.

Alexander Q. Anderson received his BS degree in optical engineering from University of Rochester and is currently a PhD student at University of Colorado Boulder. His current research interests include remote sensing, structured illumination, and orbital angular momentum.

Joseph M. Howard received a BS degree in physics from the US Naval Academy in Annapolis, Maryland, and his PhD in optical design from The Institute of Optics, University of Rochester, in Rochester, New York. He now serves as an optical designer for NASA, working on projects including the James Webb Space Telescope and the other future space missions.

Garrett West is a senior optical engineer and optical designer at Ball Aerospace in Boulder, CO. He designs and analyzes the next generation of space optical instruments and telescopes. He is optical engineering experience spans from small internal research efforts to large international missions, such as the James Webb Space Telescope. His research focus is in freeform optics, where he investigates designs with reduced volume, fewer mirrors, wider fields of view, and better image quality to meet the growing needs of aerospace missions.

Dae Wook Kim is an assistant professor of optical sciences and astronomy at the University of Arizona. His research area covers precision optical engineering, including interferometry and deflectometry. He is the chair of the Optical Manufacturing and Testing (SPIE) and Optical Fabrication and Testing (OSA) conferences. He is a senior member of OSA and SPIE and has served as an associate editor for the OSA *Optics Express* journal.